April 2013. Vol. 3, No. 2 ISSN2305-8269
International Journal of Engineering and Applied Sciences

www.eaas-journal.org

DEVELOPMENT OF AN ESTIMATION METHOD FOR INTERIOR TEMPERATURE DISTRIBUTION IN LIVE BIOLOGICAL TISSUES OF DIFFERENT ORGANS

Shazzat Hossain and F. A. Mohammadi

Department of Electrical and Electronic Engineering
Ryerson University, Toronto, ON

ABSTRACT

In worm blooded bodies, the anatomy of a superficial organ controls the influences of the volumetric heat generation rate, the perfusion rate and the heat losses rate especially due to convection and radiation on the tissue temperature. With considering the organ's physical structure and basis on the Pennes' bioheat transfer equation, a one-dimensional bioheat transfer model of living tissues in the steady state have been set up for application in different body organ's heat transfer study, and by using either the particular solution or Bessel's equation their corresponding analytic solutions have been derived. The derived analytic solutions are useful to easily and accurately explore the correlation between thermal features and body anatomy, and can be extended to such applications as parameter measurement, temperature field reconstruction and clinical treatment. The obtained results are also validated by numerical methods.

Keywords: Electronic engineering, interior temperature, Pennes' bioheat transfer equation

1. Introduction

In living bodies, heat transfer plays an important role in many physiological processes as it affects the temperature and its spatial distribution in tissues. Advances in the research of bioheat transfer paved the way to the developments in diverse areas such as hyperthermia cancer therapy, thermal diagnosis, cryogenic surgery etc. [1, 2]. The prerequisite for further quantitative and accurate analysis of bioheat transfer is to effectively understand and model the transfer mechanism of mass and energy in the biological system.

Thermal energy transfer in living tissues is a complex process which includes conduction, convection, radiation, interior metabolism, evaporation, phase change, and inherent temperature regulation. Furthermore, heterogeneity of living tissues and discrepancies in biological materials biothermal behavior have a remarkable effect of blood perfusion on the temperature field in body, which varies among different tissues and organs. Therefore, it is very difficult to build generally applicable models to precisely describe the heat transfer process, and most of the proposed bioheat equations are very complicated. Generally, the complexity of the bioheat transfer equations makes it difficult to obtain their analytic solutions.

However, analytical solutions of these equations, if attainable, are of important significance in the study of bioheat transfer because they can not only accurately reflect the actual physical feature of equations but also be used as standards to verify the corresponding results of numerical calculation. Various techniques have been proposed to obtain analytical solutions of the equations. Shitzer [3] presented and discussed the solutions for models of living tissue cooled at the skin surface. Bardati [4]

linearised and solved the non-linear operator equation for microwave hyperthermia treatments. Analytical solution also depends on bioheat equation and boundary conditions. T. C. Shih et al. [5] presented the solution of the Pennes bioheat equation with sinusoidal heat flux on skin boundary. The same bioheat equation was solved in [6] for spatial or transient heating boundary. All of the above mentioned analyses were performed in rectangular pyramidal tissue model.

However, the organs in human body have different physical structure. For example, the hand and leg are almost cylindrical, the back and male chest are close to solid rectangle and likewise buttock and female breast can be approximated as sphere. Depending on the geometry the volumetric heat generation rate and perfusion rate and the surface area over which convection and radiation heat losses occur would be changed. Therefore the temperature distribution in tissue inside would vary from organ to organ. Kai YUE solved the problem for cylindrical tissues [7] while Zhou Minhua et al [6] used rectangular pyramidal tissues.

The objective of this study is to develop a model of live organs considering their physical structure and solve the second order heat temperature equation with non-linear boundary conditions to estimate the radial flow of temperature. However the analysis includes the analytical solution of the steady-state bioheat equation with total heat exchange at skin surface has been discussed, and its corresponding numerical solution and the application of analytical results to determine some biothermal parameter's effect on thermal distribution.

2. The Bioheat Equation

Pennes' developed a bio-heat model considering blood perfusion and artier blood temperature effect on in-tissue temperature distribution which is presented as:

$$\rho c\, dT/dt = k\nabla^2 T + \omega_b c_b (T_a - T) + Q_m \qquad (1.1)$$

where ρ and c refer to the density and specific heat of tissue, respectively, ω_b is the product of blood density and perfusion rate per unit volume of tissue, c_b is the specific heat of blood, T_a is the artier blood temperature and Q_m is the rate of metabolic heat generation per unit volume of tissue.

In particular tissue, the temperature flow is controlled by the blood circulation rate, metabolism and thermal conductivity. Changes in any of these parameters, most likely for tumour, can induce variation in flow rate and spatial distribution of temperature and heat flux at skin surface. However, the transient temperature term of the Equation (1.1) has been neglected because of the time independency of other bio-thermal parameters in the equation. Therefore the steady-state form of the bio-heat equation along with suitable boundary conditions can provide spatial temperature distribution inside tissues.

However, the prominent heat flow occurs in the radial direction of an organ and involves choosing appropriate coordinate systems while solving the problem analytically. Therefore, the formulation for steady-state heat equation and boundary conditions in three different coordinate systems become the following.

For rectangular pyramidal tissues,

$$k\,(d^2 T)/〚dx〛^2 + \omega_b c_b (T_a - T) + Q_m = 0 \qquad (1.2)$$

For cylindrical tissues,

$$1/\rho \; d/d\rho\,(\rho\, dT/d\rho) + (\omega_b c_b)/k\,(T_a - T) + Q_m/k = 0 \qquad (1.3)$$

Similarly for spherical tissues,

$$1/r^2 \;\; d/dr\,(r^2 \;\; dT/dr) + (\omega_b c_b)/k\,(T_a - T) + q_m/k = 0 \qquad (1.4)$$

And the generalized boundary conditions are:

n=0, dT/dn=0 (1.5-a)

n=L, -k dT/dn=h_a (T-T_e) (1.5-b)

where, L is the thickness of the concerned tissue; h_a is the total heat exchange coefficient which accounts for both the convection and radiation heat loss on the tissue surface; T_e is the ambient temperature; n is the radial direction, for example, x-for rectangular tissues, ρ-for cylindrical tissues and r- for spherical tissues.

3. Physical Model

The temperature flow in the flat body part (such as back and male chest, can be approximated as a 3-D rectangular box, Figure 1) governs by the heat equation in (1.2) and boundary conditions in (1.5).

It is assumed that the core plane hold at the constant artier temperature and according to the boundary conditions, it is thermally insulated and the heat flux at the skin surface is fully exchange with environment. Further assuming the prominent in x-direction, the one-dimensional steady-state Pennes' bio-heat equation can be written as:

(d^2 T)/〖dx〗^2 -αT=-β (1.6)

Fig 1 Rectangular pyramidal tissue model

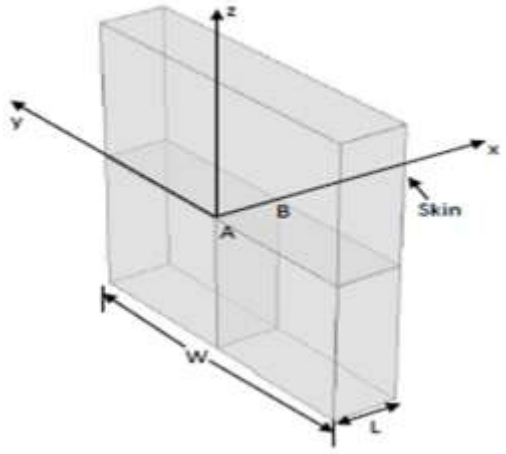

where α=(ω_b c_b)/k and β=(ω_b c_b T_a+Q_m)/k. The general solution of Equation (1.6) is obtained as:

$$T(x) = C_1 e^{-\alpha x} + C_2 e^{\alpha x} + \frac{\beta}{\alpha} \qquad (1.7)$$

The evaluation of arbitrary constants C_1 and C_2 is determined using the following boundary conditions. Thus the solution becomes,

International Journal of Engineering and Applied Sciences

www.eaas-journal.org

$$T(x) = \frac{\frac{h_a}{k}\left(T_e - \frac{\beta}{\alpha}\right)\cosh(\sqrt{\alpha}x)}{\sqrt{\alpha}\,sinh(\sqrt{\alpha}d) + \frac{h_a}{k}\cosh(\sqrt{\alpha}d)} + \frac{\beta}{\alpha} \qquad (1.8)$$

Therefore, the equation (1.8) provides the temperature flow along the line AB for the rectangular tissues.

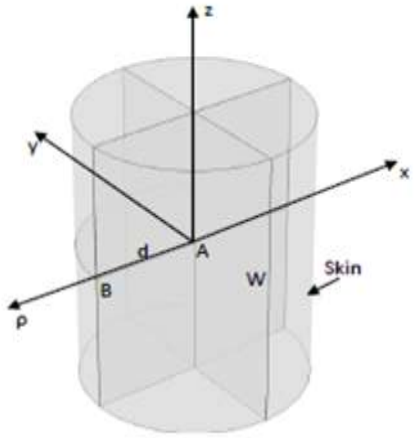

Accordingly, the cylindrical tissues (i.e. tissues in arm, forearm, leg etc.) in Fig 2 govern by the one-dimensional equation 1.3 which describes the heat transfer in such tissues in the steady-state.

To derive the radial heat flow along the line AB, the nondimensionalizations of the Equation 1.3 and its boundary conditions have been performed by the following characteristic quantities:

$$\rho^* = \frac{\rho}{L}, \qquad T^* = \frac{T - T_e}{T_a - T_e} \qquad (1.9)$$

Then, substituting (1.9) back into Equation (1.3) leads to:

$$\frac{1}{\rho^*}\frac{d}{d\rho^*}\left(\rho^*\frac{dT^*}{d\rho^*}\right) + \frac{\omega_b c_b \rho^2}{k}(1 - T^*) + \frac{Q_m \rho^2}{k(T_a - T_e)} = 0 \qquad (1.10)$$

Therefore the dimensionless parameters and variables are defined as:

$$\omega_b^* = \frac{\omega_b c_b d^2}{k}, \qquad Q_m^* = \frac{Q_m d^2}{k(T_a - T_e)}, h_a^* = \frac{h_a d}{k} \qquad (1.11)$$

Hence, the original dimensional equation and the boundary conditions can be rewritten as:

$$\frac{1}{\rho^*}\frac{d}{d\rho^*}\left(\rho^*\frac{dT^*}{d\rho^*}\right) - \omega_b^* T^* + \omega_b^* + Q_m^* = 0 \qquad (1.12)$$

And

$$\begin{cases} \rho^* = 0, & \frac{dT^*}{d\rho^*} = 0 \\ \rho^* = 1, & \frac{dT^*}{d\rho^*} = -h_a^* T^* \end{cases} \qquad (1.13)$$

In addition, in order to standardize the equation, we assume:

$$A = \omega_b^* + Q_m^*, \quad B = \omega_b^*, \quad \emptyset = A - BT^* \qquad (1.14)$$

Thus substituting (1.14) into Equation (1.12), we obtain

$$\frac{d^2\emptyset}{d\rho^{*2}} + \frac{1}{\rho^*}\frac{d\emptyset}{d\rho^*} - B\emptyset = 0 \qquad (1.15)$$

Equation (1.15) is a zero order modified Bessel differential equation, whose general solution can be expressed as:

$$R(z) = C_1 I_v(z) + C_2 K_v(z) \qquad (1.16)$$

where 〖I〗_v and K_v are the modified Bessel functions of the second kind. In order to determine if the analytic solution can be expressed by Bessel functions, Equation (1.15) has been compared with the Generalized Bessel's equation as follows:

International Journal of Engineering and Applied Sciences

www.eaas-journal.org

$$\frac{d^2R}{dx^2}+\left[\frac{1-2m}{x}-2\alpha\right]\frac{dR}{dx}+\left[p^2a^2x^{2p-2}+\alpha^2+\frac{\alpha(2m-1)}{x}+\frac{m^2-p^2v^2}{x^2}\right]R=0 \quad (1.17)$$

The corresponding solution of Equation (1.17) is:

$$R=x^m e^{ax}[C_1J_v(ax^p)+C_2Y_v(ax^p)] \quad (1.18)$$

where J_v and Y_v are the modified Bessel function of the first kinds respectively, C_1 and C_2 are arbitrary constants which can be obtained according to the given boundary conditions. The result of comparison between equation (1.15) and (1.18) is shown below:

$$\alpha=0, m=0, v=0, p=1, a^2=-B$$

Hereby, the solution of the Equation (1.17) can be expressed as:

$$\emptyset=C_1I_0(\sqrt{B}\rho^*)+C_2K_0(\sqrt{B}\rho^*) \quad (1.19)$$

Substituting (1.19) into (1.15), the solution for T^* can be written as:

$$T^*=\frac{\omega_b^*+Q_m^*}{\omega_b^*}-\left[\frac{C_1}{\omega_b^*}I_0(\sqrt{\omega_b^*}\rho^*)+\frac{C_2}{\omega_b^*}K_0(\sqrt{\omega_b^*}\rho^*)\right] \quad (1.20)$$

The next step is to determine the values of two arbitrary constants C_1 andC_2. According to the characteristics of Bessel's equation, when $z=0$, we have $I_1(0)\equiv 0$ and $K_1(0)\to\infty$. Considering the boundary conditions in Equation (1.13), and after derivations of (1.20), lead to:

$$C_2\equiv 0, \qquad \frac{dT^*}{d\rho^*}=-\frac{\sqrt{\omega_b^*}C_1}{\omega_b^*}I_1(\sqrt{\omega_b^*}\rho^*)$$

Putting $\rho^*=1, \frac{dT^*}{d\rho^*}=-h_a^*T^*$, we get:

$$-h_a^*\left(\frac{\omega_b^*+Q_m^*}{\omega_b^*}-\frac{C_1}{\omega_b^*}I_0(\sqrt{\omega_b^*})\right)=-\frac{\sqrt{\omega_b^*}C_1}{\omega_b^*}I_1(\sqrt{\omega_b^*})$$

$$C_1=\frac{h_a^*(\omega_b^*+Q_m^*)}{h_a^*I_0(\sqrt{\omega_b^*})+\sqrt{\omega_b^*}I_1(\sqrt{\omega_b^*})}$$

So we have:

$$T^*(\rho^*)=\frac{\omega_b^*+Q_m^*}{\omega_b^*}-\frac{h_a^*(\omega_b^*+Q_m^*)}{\omega_b^*[h_a^*I_0(\sqrt{\omega_b^*})+\sqrt{\omega_b^*}I_1(\sqrt{\omega_b^*})]}I_0(\sqrt{\omega_b^*}\rho^*)$$

$$T^*(\rho^*)=\frac{\omega_b^*+Q_m^*}{\omega_b^*}\left[1-\frac{h_a^*}{[h_a^*I_0(\sqrt{\omega_b^*})+\sqrt{\omega_b^*}I_1(\sqrt{\omega_b^*})]}I_0(\sqrt{\omega_b^*}\rho^*)\right]$$

$$T^*(\rho^*)=\frac{\omega_b^*+Q_m^*}{\omega_b^*}\left[1-\frac{I_0(\sqrt{\omega_b^*}\rho^*)}{\left[I_0(\sqrt{\omega_b^*})+\frac{\sqrt{\omega_b^*}}{h_a^*}I_1(\sqrt{\omega_b^*})\right]}\right]$$

Finally analytical solution for T is given by:

$$T=T_e+(T_a-T_e)\frac{\omega_b^*+Q_m^*}{\omega_b^*}\left[1-\frac{I_0(\sqrt{\omega_b^*}\rho^*)}{\left[I_0(\sqrt{\omega_b^*})+\frac{\sqrt{\omega_b^*}}{h_a^*}I_1(\sqrt{\omega_b^*})\right]}\right]$$

$$T=T_e+(T_a-T_e)\left[1+\frac{Q_m}{\omega_b c_b(T_a-T_e)}\right]\left[1-\frac{I_0\left(\sqrt{\frac{\omega_b c_b}{k}}\rho\right)}{\left[I_0\left(\sqrt{\frac{\omega_b c_b d^2}{k}}\right)+\frac{k\sqrt{\omega_b^*}}{h_a d}I_1\left(\sqrt{\frac{\omega_b c_b d^2}{k}}\right)\right]}\right] \quad (1.21)$$

The equation (1.21) expresses the radial heat flow in cylindrical living tissues.

International Journal of Engineering and Applied Sciences

www.eaas-journal.org

Likewise the physical model of spherical live biological tissues at steady-state condition proposed in Figure 3.

To obtain the dimensionless heat equation and boundary conditions the following characteristics quantities are considered.

$$r^* = \frac{r}{R}, \qquad T^* = \frac{T - T_e}{T_a - T_e} \qquad (1.22)$$

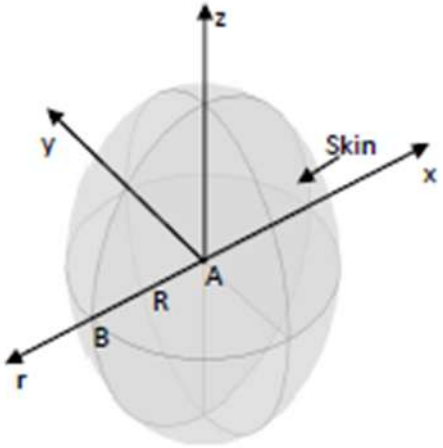

Fig 3 Spherical tissue model

Using the Equation 1.22 the Equation 1.4 can be written as:

$$\frac{1}{r^{*2}}\frac{d}{dr^*}\left(r^{*2}\frac{dT^*}{dr^*}\right) + \frac{\omega_b c_b R^2}{k}(1 - T^*) + \frac{q_m R^2}{k(T_a - T_e)} = 0 \qquad (1.23)$$

and the dimensionless boundary conditions are:

$$r^* = 0, \qquad \frac{dT^*}{dr^*} = 0 \qquad (1.24 - a)$$

and

$$r^* = 1, \qquad \frac{dT^*}{dr^*} = -\frac{h_a R}{k}T^* \qquad (1.24 - b)$$

The dimensionless parameters and variables are defined as:

$$\frac{\omega_b c_b R^2}{k} = \omega^*, \frac{q_m R^2}{k(T_a - T_e)} = q_m^* \text{ and } \frac{h_a R}{k} = h_a^*$$

Therefore, the dimensionless governing equation is:

$$\frac{1}{r^{*2}}\frac{d}{dr^*}\left(r^{*2}\frac{dT^*}{dr^*}\right) - \omega_b^* T^* + \omega_b^* + q_m^* = 0 \ (1.24)$$

and the boundary conditions are:

$$r^* = 0, \qquad \frac{dT^*}{dr^*} = 0 \qquad (1.26 - a)$$

and

$$r^* = 1, \qquad \frac{dT^*}{dr^*} = -h_a^* T^* \qquad (1.26 - b)$$

By dropping the superscripts * and letting $\omega_b^* = \alpha$ and $\omega_b^* + q_m^* = \beta$, the equation (1.25) becomes:

$$\frac{1}{r^2}\frac{d}{dr}\left(r^2\frac{dT}{dr}\right) - \alpha T + \beta = 0 \qquad (1.27)$$

To solve the equation (1.27), let's assume $T = \frac{H_{(r)}}{\sqrt{r}}$ and by differentiating we obtain,

$$\frac{dT}{dr} = \frac{1}{\sqrt{r}}H' - \frac{1}{r\sqrt{r}}H \qquad (1.28)$$

Substituting (1.28) in (1.27) we obtain,

$$\frac{1}{r^2}\frac{d}{dr}\left(r\sqrt{r}H' - \frac{1}{2\sqrt{r}}H\right) - \frac{\alpha}{\sqrt{r}}H = -\beta \qquad (1.29)$$

The homogeneous equation is:

$$\frac{1}{r^2}\frac{d}{dr}\left(r\sqrt{r}H' - \frac{1}{2\sqrt{r}}H\right) - \frac{\alpha}{\sqrt{r}}H = 0 \qquad (1.30)$$

After simplifying and multiplying by $\sqrt{r}$, we obtain

$$r^2H'' + rH' - \left(\alpha r^2 + \left(\frac{1}{2}\right)^2\right)H = 0 \qquad (1.31)$$

The equation (1.31) is modified Bessel equation of half kind and therefore the solution is:

$$H = C_1 I_{1/2}\left(\sqrt{\alpha}r\right) + C_2 K_{1/2}\left(\sqrt{\alpha}r\right) \qquad (1.32)$$

According to the characteristics of Bessel's equation, we have $C_2 = 0$. Therefore, the solution to (1.32) is:

$$H = C_1 I_{1/2}\left(\sqrt{\alpha}r\right) \qquad (1.33)$$

The exact solution in terms of $T(r)$ is:

International Journal of Engineering and Applied Sciences

www.eaas-journal.org

$$T = C_1 \frac{I_{1/2}(\sqrt{\alpha} r)}{\sqrt{r}} + T_p \qquad (1.34)$$

where, T_p is the particular solution and $T_p = \frac{\beta}{\alpha}$. Therefore, the temperature expression considering the superscript * again:

$$T^*(r^*) = C_1 \frac{I_{1/2}(\sqrt{\alpha} r^*)}{\sqrt{r^*}} + \frac{\beta}{\alpha} \qquad (1.35)$$

Considering the boundary condition of (1.26-b), and after derivations of (1.35) lead to:

$$\frac{dT^*}{dr^*} = C_1 \left(-\frac{I_{1/2}(\sqrt{\alpha} r^*)}{2r^* \sqrt{r^*}} + \frac{\sqrt{\alpha} I_{3/2}(\sqrt{\alpha} r^*) + \frac{1}{2r^*} I_{1/2}(\sqrt{\alpha} r^*)}{\sqrt{r^*}} \right) \qquad (1.36)$$

$$C_1 \left(-0.5 I_{1/2}(\sqrt{\alpha}) + \sqrt{\alpha} I_{3/2}(\sqrt{\alpha}) + 0.5 I_{1/2}(\sqrt{\alpha}) \right) = -h_a^* \left(C_1 I_{1/2}(\sqrt{\alpha}) + \frac{\beta}{\alpha} \right) \qquad (1.37)$$

$$C_1 = \frac{-h_a^* \frac{\beta}{\alpha}}{\sqrt{\alpha} I_{3/2}(\sqrt{\alpha}) + h_a^* I_{1/2}(\sqrt{\alpha})}$$

$$T^* = \frac{-h_a^* \frac{\beta}{\alpha}}{\sqrt{\alpha} I_{3/2}(\sqrt{\alpha}) + h_a^* I_{1/2}(\sqrt{\alpha})} \frac{I_{1/2}(\sqrt{\alpha} r^*)}{\sqrt{r^*}} + \frac{\beta}{\alpha}$$

$$T^* = \frac{\beta}{\alpha} \left[1 - \frac{h_a^*}{\sqrt{\alpha} I_{3/2}(\sqrt{\alpha}) + h_a^* I_{1/2}(\sqrt{\alpha})} \frac{I_{1/2}(\sqrt{\alpha} r^*)}{\sqrt{r^*}} \right]$$

$$T = T_e + \frac{\beta}{\alpha} \left[1 - \frac{h_a^*}{\sqrt{\alpha} I_{\frac{3}{2}}(\sqrt{\alpha}) + h_a^* I_{\frac{1}{2}}(\sqrt{\alpha})} \frac{I_{\frac{1}{2}}(\sqrt{\alpha} r^*)}{\sqrt{r^*}} \right] * (T_a - T_e) \qquad (1.38)$$

Therefore the Equation 1.38 provides the analytical solution for the temperature profile in tissue interior of spherical tissues.

4. Numerical Model

The numerical models of the living tissues of the above mentioned organs have been presented in order to validate the obtained analytical solution in section 3. The models were developed and analyzed using numerical analysis software, the COMSOL [10] multiphysiscs.

The COMSOL solver is powerful and popular numerical analysis software which works based on the finite element method. The solver featured with an environment to analyze the heat transfer in Biological tissues which has been applied to estimate the internal temperature profiles of different types of living tissues. The stationary simulation process requires performing several steps including the geometry design, mesh formation, parameters and boundary settings.

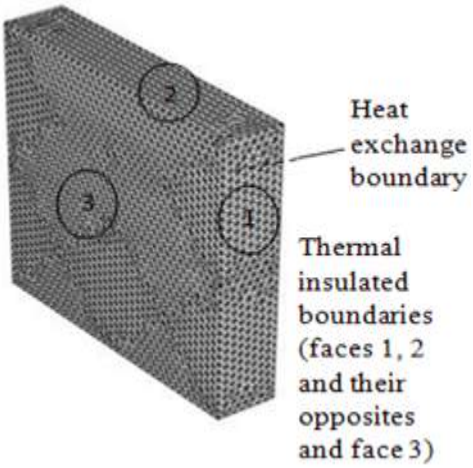

(A)

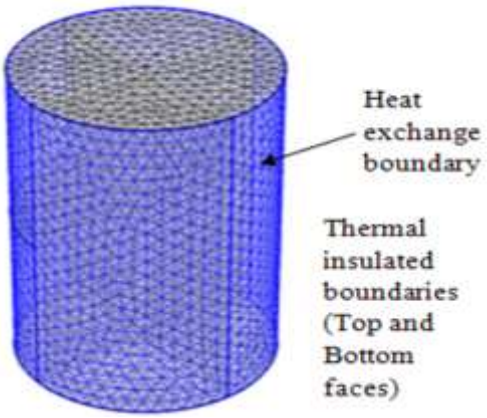

(B)

International Journal of Engineering and Applied Sciences

www.eaas-journal.org

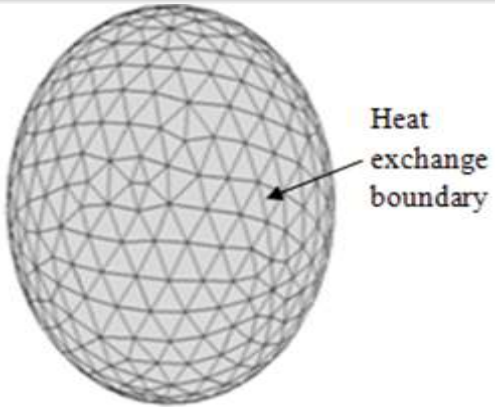

(C)

Fig 4 Numerical models for (a) Rectangular, (b) Cylindrical and (c) Spherical tissues

In geometry design the physical models in Figures 1 through 3 have been considered. We assume the dimension 4 cm×10 cm×10 cm for the rectangular pyramidal tissues, the radius 4 cm and height 10 cm for the cylindrical tissues and the radius 4 cm for the spherical tissues. Therefore for each case the tissue thickness is 4 cm (indicates line AB). The most convenient way to acquire radial tissue temperature is dividing the models into several segments (see Figure 1 to 3) and compute temperature along line AB. For that reason, we define three rectangles and extrude them in z-axis to develop the rectangular pyramidal model and also extrude six quarter circles in z-axis for the cylindrical model. However two quarter circles are revolved around z-axis to obtain the spherical model.

The mesh structures of the models are shown in Figure 4. In Figure 4(a), the mesh layout of rectangular box model, the superficial boundary z = 0.04 is the skin surface and assumed to heat loss surface and the remaining five faces are thermally insulated. Accordingly, the mesh structure of cylindrical model, in Figure 4(b) has the heat exchange surface at ρ=0.04 and both the top and bottom circular surfaces are thermally isolated. However, for Figure 4(c) the sphere periphery is assumed exchanging heat with environment.

In addition, the entire domain of the rectangular pyramidal model was divided into approximately 27000 tetrahedral and 3500 triangular elements. In the cylindrical tissues, the domain was composed of more than 200,000 tetrahedral elements and 28,000 triangular elements. Similarly for spherical organs, the tissues were divided into approximately 5060 tetrahedral and 800 triangular elements. Numerous iterations of mesh refinement were performed to determine the maximum and minimum element sizes in order to obtain a good resolution in the simulated patterns, and to minimize the computational memory and simulation time. In addition, nodes along the surface area constrained in the normal-translational direction for all three geometries. All other nodes are unconstrained in all directions. A constant temperature of 20 oC was applied at the entire section as an initial condition. The maximum and minimum element sizes are chosen as 0.6 and 0.2 mm, respectively. The maximum element aspect ratio is 1.5.

The 'Stationary' analysis has been performed for steady-state thermal analysis.

5. Results and Discussion

The analytic results obtained using MATLAB and the numerical results obtained from COMSOL have been presented abreast to show a clear comparison between them. For both analyses the values of the thermal parameters have been used is listed in Table 1.

The analytic solutions in Equations (1.8), (1.21) and (1.38), respectively for the rectangular, cylindrical and spherical tissues and their respective numerical solutions are presented in Figure 5.

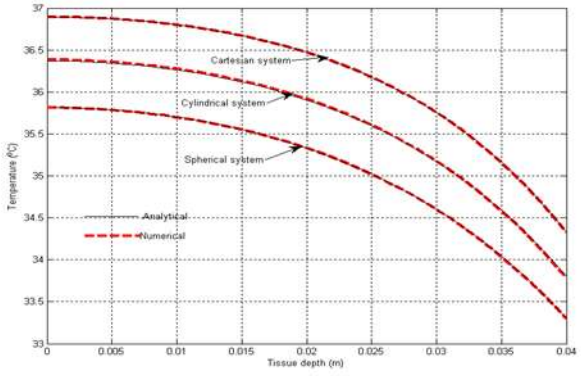

Fig 5 Tissue temperature profiles

International Journal of Engineering and Applied Sciences

www.eaas-journal.org

Table 1: Thermo-physical parameters

Parameter	Symbol	Value	Unit
Thermal	k	0.51	W m^{-1} $^0C^{-1}$
Heat Exchange Coefficient	h_a	13.7	W m^2 ^0C
Specific Heat (Blood)	c_b	4186	J kg^{-1} ^0C
Density (Blood)	ρ_b	1000	Kg m^{-3}
Perfusion Rate	ω_b	5.4×10^{-4}	s^{-1}
Metabolism	Q_m	700	W m^{-3}
Tissue Thickness	x	0.04	m
Arterial Blood Temperature	T_a	37	^0C
Environment Temperature	T_e	27	^0C

The temperature curves indicate that the flat organ's tissues have higher temperature than the tubular and curved organs. Therefore the box organs may be the warmest parts of human body have roughly 1oC higher surface temperature than the spherical part or 0.5oC higher than the cylindrical part.

In addition, the analysis also make it evident that in identical ambient condition and if all biothermal parameters remain the same then the temperature on human back or a male chest will have higher value than that of on the forearm or female breast. It may be due to the relatively smaller surface area over which heat loss occurs for an equal volume flat organ.

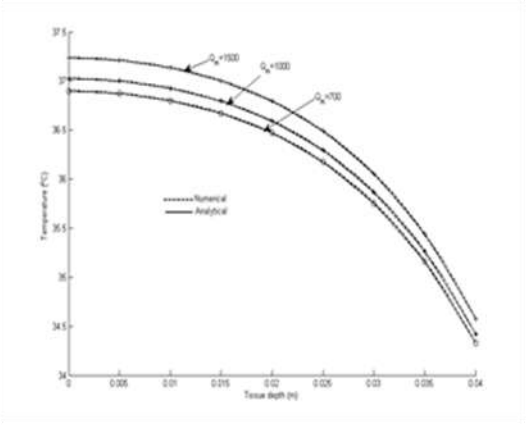

(a)

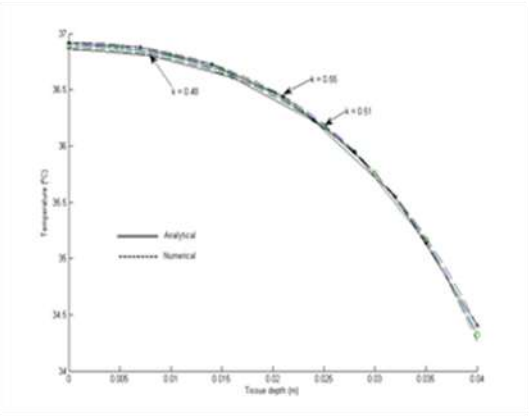

(b)

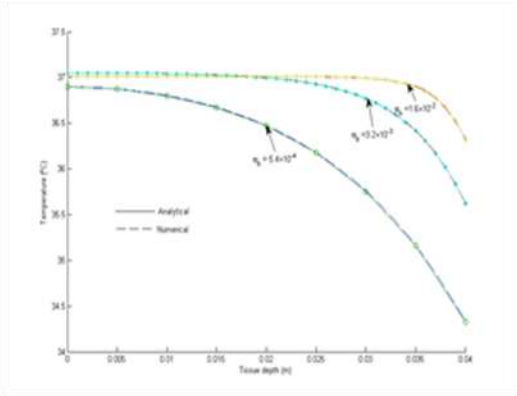

(c)

Fig 6 Effect of biological parameter on temperature profile in rectangular tissue –influence of (a) Metabolic heat generation, (b) Thermal conductivity and (c) Blood perfusion

International Journal of Engineering and Applied Sciences

www.eaas-journal.org

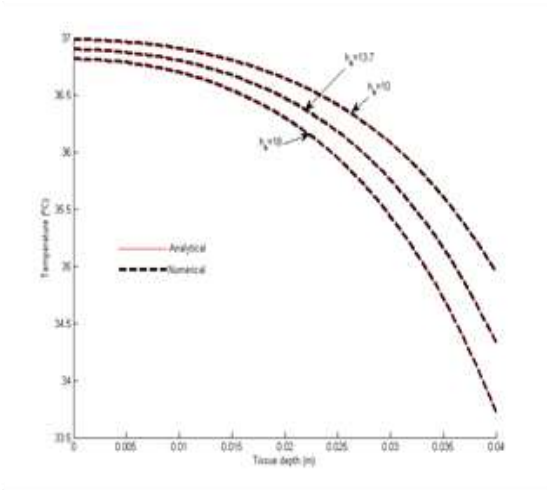

(a)

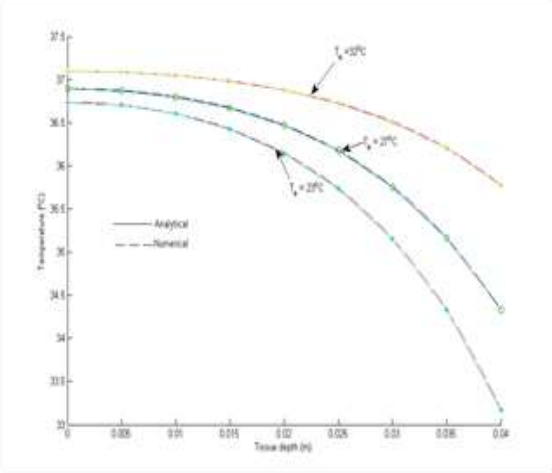

(b)

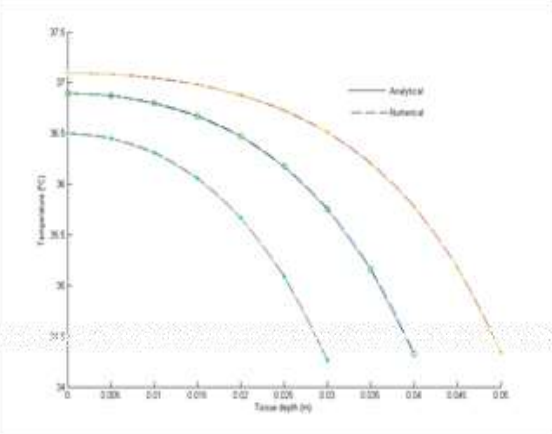

(c)

Fig 7 Effect of ambient conditions and model thickness on temperature distribution – (a) Heat exchange rate, (b) Ambient temperature and (c) Tissue thickness

The analysis has also been performed to estimate the influences of the bio-thermal and physical parameters on the tissue temperature. The Figure 6 shows the effect of some biological parameters on the temperature distribution of rectangular pyramidal tissues. The Figure 6(a) showed, how the tissue temperature has been affected by the change in metabolic heat generation.

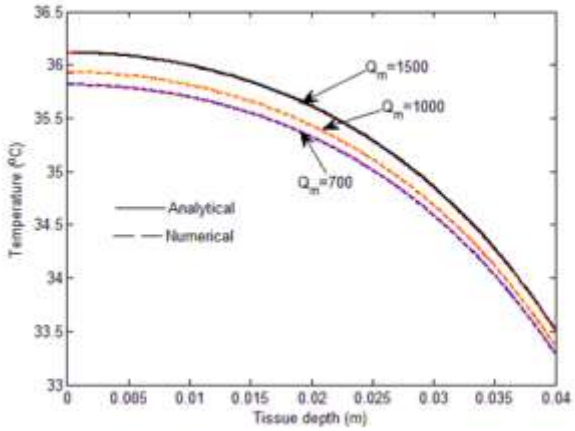

(8a)

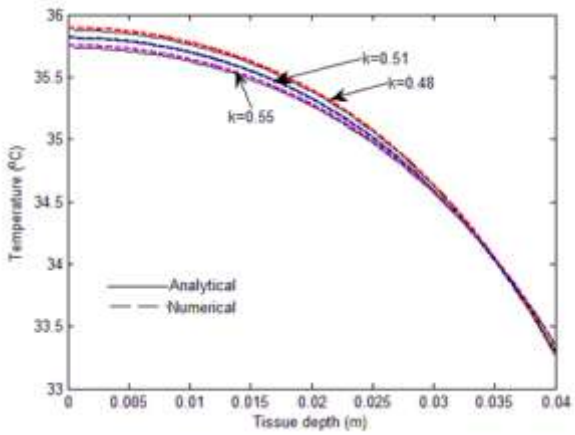

(8b)

International Journal of Engineering and Applied Sciences

www.eaas-journal.org

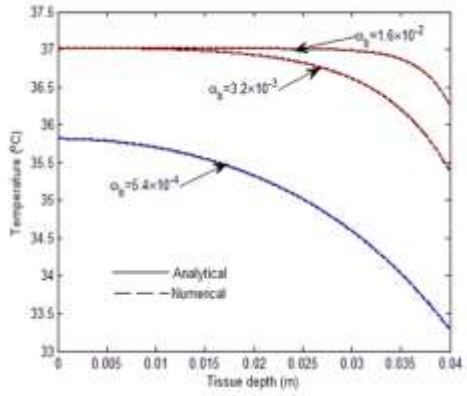

(8c)

Fig 8 Effect of biological parameter on temperature profile in cylindrical tissue –influence of (a) Metabolic heat generation, (b) Thermal conductivity and (c) Blood perfusion

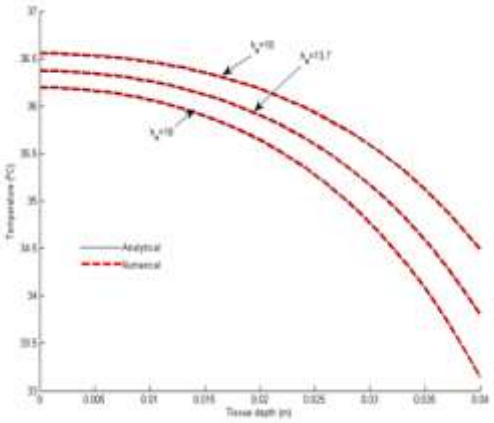

(9a)

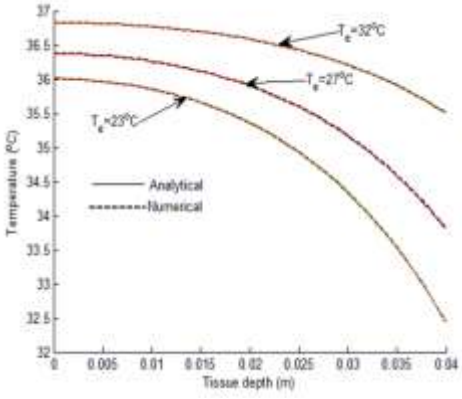

(9b)

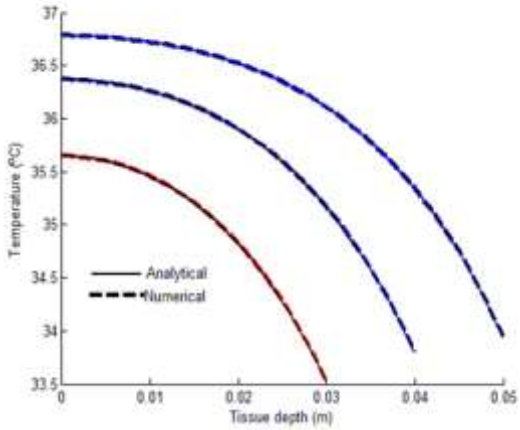

(9c)

Fig 9 Effect of ambient conditions and model thickness on temperature distribution – (a) Heat exchange rate, (b) Ambient temperature and (c) Tissue thickness

If the metabolic rate changed from 700 W/m3 to 1500 W/m3 the skin temperature increased by almost 0.1oC. The Figure 6(b) indicates that the thermal conductivity has insignificant effect on the temperature distribution as it varied between 0.48 and 0.55 W m-1 0C-1.

In comparison with the case of blood perfusion of (w=5.4×10-4 1/s), it is obvious that the increase of blood perfusion has a remarkable influence on the surface temperature in living tissues as shown in Fig. 6c. The curves in Fig 6.c indicate that the gradient of the temperature variation in radial direction decreases with increasing blood perfusion, which is a result of higher rate of heat distribution caused by the blood perfusion. In addition, the differences between the effects of the higher blood perfusion rates on temperature distributions become smaller. The core temperature approaches to a constant value of 37oC.

The effect of the ambient condition, for example, the heat loss rate and environment temperature on the temperature distribution in rectangular tissue have been presented in Figure 7(a) and (b), respectively. Both figures indicate that the ambient conditions have significant effects on the surface temperature. Therefore a controlled environment might play an important role in the hyperthermia diagnosis process.

International Journal of Engineering and Applied Sciences

www.eaas-journal.org

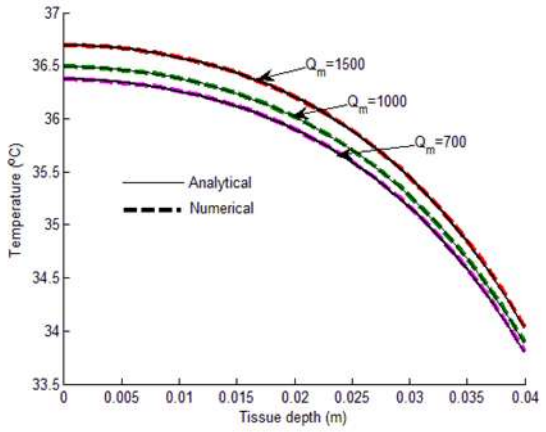

(10a)

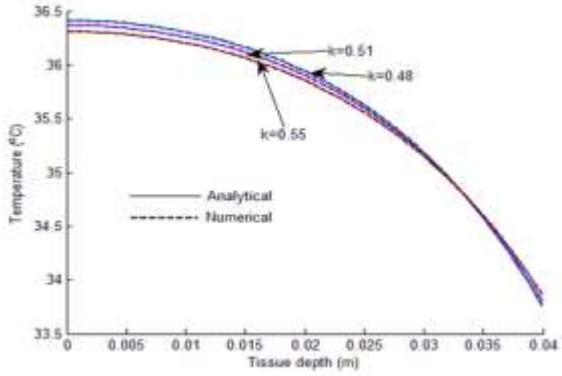

(10b)

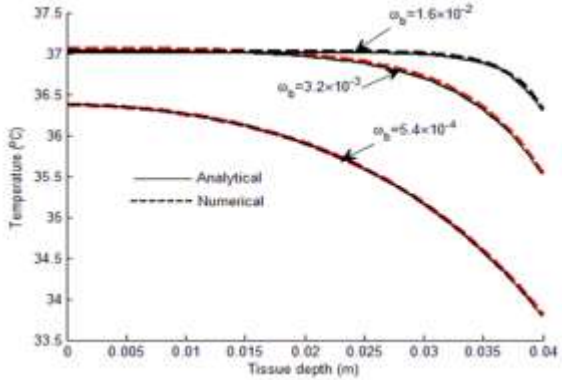

(10c)

Fig 10 Effect of biological parameter on temperature profile in cylindrical tissue –influence of (a) Metabolic heat generation, (b) Thermal conductivity and (c) Blood perfusion

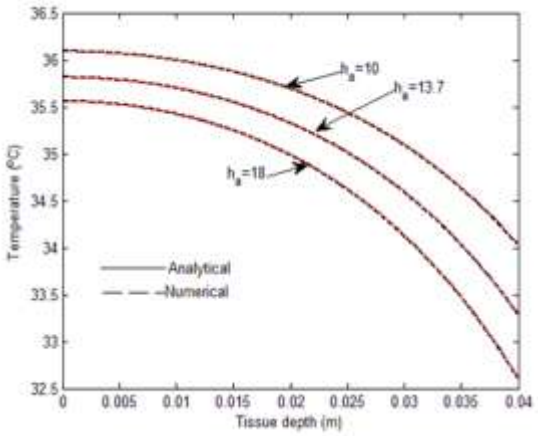

(11a)

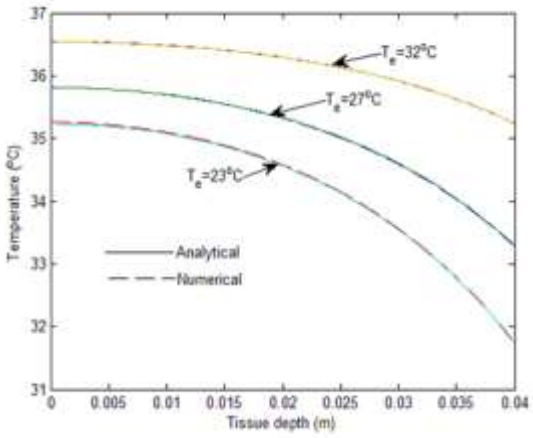

(11b)

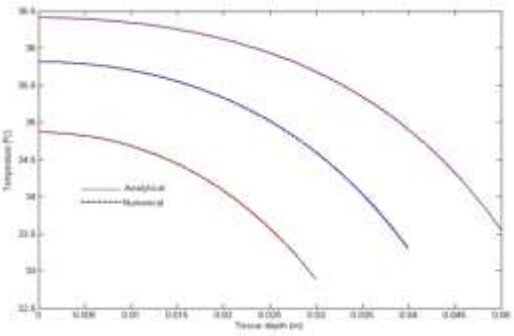

(11c)

International Journal of Engineering and Applied Sciences

www.eaas-journal.org

Fig 11 Effect of ambient conditions and model thickness on temperature distribution – (a) Heat exchange rate, (b) Ambient temperature and (c) Tissue thickness

The effect of tissue thickness on the temperature profile is also presented in Figure 7(c) where it is seen that tissue thickness has no effect on the surface temperature.

The similar analyses have been conducted on the cylindrical and spherical tissues which are presented in Figures 8 through 11. The figures indicate that the profiles flow the similar behaviour of the rectangular tissues and the only inconsistency has been found for the temperature versus tissue thickness curve. Unlike the rectangular tissues the cylindrical and spherical organ's thickness have a little influence on the surface temperature.

The Figures 5 to 11 show that the derived analytical solutions comply with their respective numerical solutions. Therefore the obtained analytical solution is a suitable alternative tool for thermal analysis of living tissues located on different organs in human body. Consequently the further analysis has performed to provide some useful information about parameter's effect on temperature distribution that can be applied to estimate the thermo-physical effect of a tumour. The heat conductivity, metabolic heat generation and blood perfusion rate could be affected in case of tumour

6. Conclusion

In this paper the analytical solution of one dimensional steady-state Pennes' bio-heat model has been derived for rectangular pyramidal, cylindrical and spherical living tissues. The analytic solution expressed by the exact solution for rectangular tissues and by the Bessel's function for cylindrical and spherical tissues is derived to obtain the temperature changes in radial direction. As a consequence, the accurate initial temperature field can be easily achieved with respect to the various transient analysis and calculation of heat transfer in living tissues.

The results given by the precise analysis has been compared to the numerical solution to demonstrate the suitability of analytical results. The analysis also shows how organ's geometry controls the temperature texture. The analysis result can also be applied to find the effect of thermal conductivity, heat generation rate, blood perfusion and heat exchange coefficient on the temperature distribution which can provide a good knowledge of thermal behaviour of living tissues. This information can be applied to measure the thermal parameters, the reconstruct the temperature field with the help of some optimization method and also can be extended for the thermal diagnosis and hyperthermia treatment.

Acknowledgement

The authors would like to acknowledge the supports provided by National Science and Engineering Research Council of Canada (NSERC) and Ryerson University.

References

a. Chato J: Measurement of thermal properties of biological materials. A Shitzer, RC. Eberhart (Eds.), Heat transfer in Medicine and biology, Plenum Press, NY, 1985, 1: 167-173.
b. Bowman HF: Estimation of tissue blood flow. A Shitzer, RC. Eberhart (Eds.), Heat transfer in Medicine and biology, Plenum Press, NY, 1985, 1: 193-230.
c. Chen MM, Pedersen CO, Chatro JC: On the feasibility of obtaining three-dimensional information from thermographic measurements. ASME Journal of Biochemical Engineering 1977, 99: 58-64.
d. Agnelli JP, Barrea AA, Turner CV: Tumor location and parameter estimation by thermography. Mathematical and Computer modeling, 2011, 53:1527-1534.
e. Ring EFJ: Progress in the measurement of human body temperature. IEEE Eng. Med. Biol. 1998, 17(4): 19-24.
f. Zhou Minhua, Chen Qian: Estimation of Temperature Distribution in Biological Tissue by Analytic Solutions to Pennes' Equation. 2nd International Conference on Biomedical Engineering and Informatics, BMEI, IEEE, 2009: 1-4.
g. Kai YUE, Xinxin ZHANG, Fan YU: An Analytic Solution of One-dimensional Steady-state Pennes' Bioheat Transfer Equation in Cylindrical Coordinates. Journal of Thermal Science, 13 (3): 255-258.

h. Deng ZS, Liu J: Mathematical modeling of temperature mapping over skin surface and its implementation in thermal disease diagnostics. Comput Biol Med 2004, 34:495-521.
i. Ng EYK, Sudharan NM: An improved tree-dimensional direct numerical modeling and thermal analysis of a female breast with tumor. Proc Inst Mech Eng Part H- J Eng Med 2001, 215: 25-37.
j. Mohammadi FA, Attar SS: Development of an Electro-thermal Simulation Tool for Integrated Circuits. Canadian Journal of Electrical and Computer Engineering, 2008, 33 (3): 191-200.
k. Ng EYK, Sudharan NM: Numerical uncertainty and perfusion induced instability in bioheat equation: its importance in thermographic interpretation. J Med Eng Tech 2001, 25: 222-229.
l. Lawson RN: Implication of surface temperatures in the diagnosis of breast cancer. Canadian Medical Association Journal 1956, 75: 309-310.
m. Lawson RN, Chugtai MS: Breast Cancer and body temperatures. Canadian Medical Association Journal 1956, 88: 68-70.
n. Diakides NA, Bronziano JD: Medical infrared imaging. Florida, USA, CRC Press, 2007.
o. Santa Cruz GA, Bertotti J, Marin J, Gonzalez SJ, Gossio S, Alvarez D, Roth BMC, Menemdez P, Pereira MD, Albero M, Cubau L, Orellano P, Liberman SJ: Dynamic infrared imaging of cutaneous melanoma and normal skin in patients treated with BNCT. Applied Radiation and Isotopes 2009, 67: 54-58.
p. Manu Mital, Ramana M. Pidaparti: Breast tumour simulation and parameters estimation using evolutionary algorithm. Hindawi publishing center, modeling and simulation in engineering, 2008, doi: 10. 1155/2008/756436.
q. Manu Mital, Scott EP: Thermal detection of embedded tumours using infrared imaging. ASME journal of biomechanical engineering, 2007, 129: 33-39.
r. Pennes HH: Analysis of tissue and arterial blood temperatures in the resting human forearm. J. Appl. Physiol. 1948, 1: 93–122.
s. L. Davis: Handbook of genetic algorithm. Van Nostrand Reinhold, New York, NY, USA; 1991.
t. Introduction to COMSOL Multiphysics, version 4.2, available online, April, 2011:http://www.comsol.com/shared/downloads/comsol_v4_building_model.pdf
u. Hossain S, Mohammadi FA, Nezad ET: Neural network approach for the determination of heat Source parameters from the surface temperature image. Proc of the 24th Canadian Conference on Electrical and Computer Engineering, 2011, 1109-1112.
v. Uyen D. Nguyen, Steven Brown J, Joseph Krycia, Mark S. Mirotznik: Numerical Evaluation of heating of the human head due to magnetic resonance imaging. IEEE transactions on biomedical engineering, 2004, 51(8): 1301-1309.
w. Goldberg DE, Genetic algorithms in search, optimization and machine learning. Addison-wesley, Reading, Mass, USA, 1989.
x. Garcia S, Guynn J, and Scott EP: Use of genetic algorithm in thermal property estimation: part II—simultaneous estimation of thermal properties. Numer Heat transfer, part A, 33(2): 149-168.
y. Miyakawa M, Bolomey JC: Non-invasive Thermometry of the human body, CRC Press, Boca Raton, 1996.